AIAA JOURNAL
Vol. 47, No. 9, September 2009

Studies on Unsteady Shock Interactions Near a Generic Scramjet Inlet

D. Mahapatra* and G. Jagadeesh†
Indian Institute of Science, Bangalore 560012, India

DOI: 10.2514/1.41954

An experimental and numerical study is presented to show the effect of cowl length and angle on the ramp/cowl shock interaction phenomena for a two-dimensional planar scramjet inlet model. Experiments are conducted in a hypersonic shock tunnel, at Mach 8, at four lengths of cowl and three cowl angles. Investigations include schlieren flow visualization near the cowl region and static pressure and heat transfer rate measurement inside the inlet chamber. Various ramp/cowl shock interaction processes resulted for different cowl configurations have been visualized using a high-speed camera. Edney type-II interference pattern is observed for 131 and 141-mm cowl lengths, whereas it is an Edney type-I interference pattern in case of a 151 mm cowl with all their typical features resulting because of the ramp/cowl shock interaction. Experiments with a cowl configuration other than 0 deg show the flow to be established through the inlet because of the reduced contraction ratio. Heat transfer peaks can be observed for the 10 and 20-deg cowl cases where flow through the inlet is found to be established. These may serve as the possible locations of fuel injection.

Nomenclature

H	=	flow enthalpy, MJ/kg
h	=	height of model, mm
l	=	length of model, mm
M	=	Mach number
p	=	pressure, Pa
Re	=	Reynolds number
T	=	temperature, K
w	=	width of model, mm
ρ	=	density, kg/m^3

Subscripts

0	=	total quantity
∞	=	freestream quantity

I. Introduction

THE shock-on-lip (SOL) condition desirable for optimum performance of the inlet is usually not satisfied for fixed geometry inlets when it is operated at off-design Mach numbers. The inlet with a variable geometry can be useful for operating in a wide range of Mach numbers. Studies on various variable-geometry configurations have been reported in the literature. Falempin and Wendling [1] have experimentally investigated the starting process for a variable-geometry air inlet operating from Mach 2 to Mach 8. Mrozinski and Hayes [2] examined a variable-geometry inlet design consisting of a cowl and a sidewall with a gap in the cowl sidewall interface. Marquart [3] performed an experimental study in a hypersonic wind tunnel on a 2-D generic hypersonic inlet for a variety of ramp angles, contraction ratios, cowl locations, and backpressures. Studies also include the use of exchangeable ramp blocks [4], and the rotation of cowl [5] to adapt the contraction ratio (CR) to a flight condition. One of the simple variable-geometry features is the variation of cowl geometry and position. The cowl can be extended upstream to reduce spillage when the inlet operates at off-design Mach numbers. The vertical position of the cowl can be varied so that the CR changes depending upon the required flight conditions. On the other hand, the cowl angle with reference to flow direction can also be varied to overcome the problem of establishment of the flow through the inlets at a given altitude. In all these cases the different cowl configurations will result in different forebody/cowl shock interactions, which directly alter the inlet characteristics. Hence it is important to understand these shock interaction processes for different cowl configurations at different experimental conditions. It is also important to evaluate whether the shock interaction processes ahead of the cowl are steady or unsteady and the corresponding implications on the flow through the inlet. There are few investigations reported in the open literature on the role of cowl on inlet performance. Kanda et al. [6] tested six inlet models in a Mach 4 wind tunnel where the parameters of studies were the side plate sweep angle, the contraction ratio, and cowl geometry. Holland [7] examined both experimentally and computationally the effects of Reynolds number and cowl position on the internal shock structure and the resulting performance of a 3-D sidewall compression scramjet inlet with leading-edge sweep of 45 deg at Mach 10. Van Wie and Ault [8] performed a combined experimental and analytical investigation to the internal flowfield of a 2-D scramjet inlet at Mach 10. The ability of the inlet to operate for a range of cowl shock positions is demonstrated. Boon and Hillier [9] performed numerical simulations for a dual mode axisymmetric hypersonic inlet for an inlet-cowl configuration at a Mach 6 centerbody-cowl design condition and at two off-design Mach numbers 5 and 7. Mouton and Hornung [10] reported experimental studies on the mechanism inducing transition between regular and Mach reflection which they performed in a Ludwieg tube. They also examined the transition due to energy deposition.

From the literature survey presented above it can be understood that little has been reported where people have made exhaustive experimental studies on the shock interaction process near an inlet particularly in an impulse facility like shock tunnel where the flow energy is also simulated in addition to the Mach–Reynolds simulation. The present investigation involves performing experimental studies mainly for two types of variable-geometry configurations, namely, varying the cowl length and varying the cowl angle keeping all other parameters constant. The discussions presented in this paper are a part of the investigation that considers shock interaction processes near a generic scramjet inlet resulting by employing a few variable geometric features both at design and off-design conditions. This paper, however, will focus on the shock interactions near the inlet resulting from the variation of the cowl length and cowl angles at

Received 1 November 2008; revision received 12 June 2009; accepted for publication 13 June 2009.

*Research Student, Aerospace Engineering Department.
†Associate Professor, Aerospace Engineering Department. Senior Member AIAA.

design condition only. In this backdrop the present investigation has the following objectives:

1) A close observation of the shock interaction processes resulting from the variation of cowl length and cowl angle to understand the flow physics.

2) Carrying out point measurements like static pressure and convective heat transfer rate inside the chamber to get an idea of the flow inside the chamber for different shock interactions ahead of the cowl.

3) Carrying out numerical studies for all cowl configurations to compliment the experiments.

II. Experimental Facility

All experiments in the present study are carried out in the Indian Institute of Science (IISc) hypersonic shock tunnel HST2. This tunnel can operate in both a straight-through mode or a reflected mode with a Mach number range of 5.75–12 and simulate flow enthalpy up to 5.0 MJ/kg for a test time of ~1 ms. It consists of a stainless-steel shock tube of 50 mm diam connected to a convergent–divergent conical nozzle of 300-mm exit diam. The hypersonic flow from this nozzle goes through a rectangular test section of 300 × 300 mm cross section and 450 mm length to a dump tank having a volume of 1 m^3. The driver and driven sections of the shock tube are separated by a metallic diaphragm of appropriate thickness and the shock tube and the nozzle are separated by a thin paper diaphragm. The flow Mach number in the test section is varied by changing the throat portion of the nozzle. A schematic diagram of this facility is given in Fig. 1. HST2 is equipped with a "z-type" schlieren imaging arrangement that include a high-speed camera (Phantom 7.2 high-speed camera, Ms. Vision Research, USA) for visualizing the flowfield of the model to be tested. For a detail description of the schlieren setup, refer to [11].

III. Test Model and Experiments in Shock Tunnel

The present model is a 2-D, planar and single ramp model designed for a Mach number of 8.0. The main reason for adopting an inlet model of 2-D planar configuration is to ensure that the model is as simple as possible so that the flow complexities due to the shape of the model can be minimized. In addition, the single ramp compression is preferred to the multiramp compression mainly due to two reasons. First, in the case of multiramp compression, the overall length of the model is too big to be accommodated in the facility. Second, is to make sure that the shock structure can be visualized. The greater the turning angle of the ramp, the stronger will be the shock coming from it and hence higher density gradient. The dimension of the model is determined from the oblique shock theory so that the SOL is satisfied at the designed Mach number for a chamber height of 10 mm. The final dimensions of the model are decided with a compromise between the theoretically obtained dimensions and the facility constraints (allowable maximum length that can be accommodated). The model has a ramp angle of 27 deg, overall length of 230 mm, and width of 112.6 mm. For the design condition, the chamber has a dimension of 85 × 100 × 10 mm ($l \times w \times h$). Various cowl configurations are fabricated and assembled to the forebody of fixed dimensions as may be required in the experiments. Figure 2 shows the schematic of the forebody-cowl configurations tested. The model is instrumented with four kulite pressure transducers (Kulite Semiconductor Product, Inc., USA) and six platinum thin-film sensors located inside the chamber for the measurement of static pressure and heat transfer rate, respectively, inside the chamber. The details of the gauge preparation and heat transfer rate reduction can be found in [12]. For the present set of experiments the high-speed

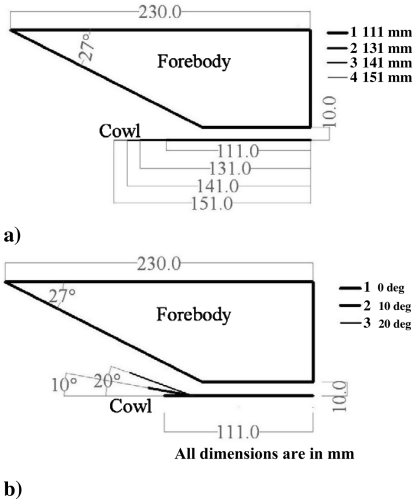

Fig. 2 Schematic of the forebody-cowl configurations tested at a) all lengths, and b) all angles.

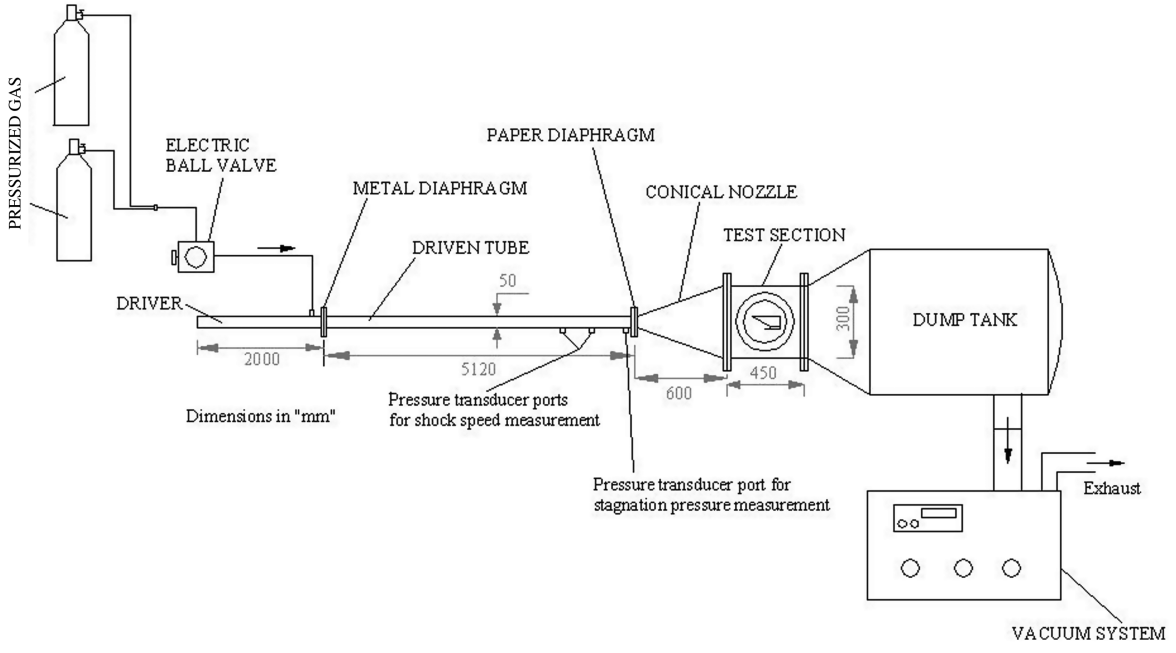

Fig. 1 Schematic diagram of the HST2 facility.

Table 1 Typical freestream conditions for the present experiments

M_∞	p_0, bar	H_0, MJ/kg	ρ_∞, Kg/m^3	p_∞, Pa	Re_∞/m	T_∞, K
7.9 (±1.0%)	22.5 (±3.0%)	2.08 (±3.2%)	0.0060 (±4.7%)	250 (±3.2%)	$1.1321e^6$ (±5.9%)	149.1 (±3.5%)

camera is operated at 10,000 frames/s with a resolution of 450 × 450 pixels and exposure time of 98 μs.

A standard 300-W North Star lamp with a *C*-clamp base is used as a continuous light source. Operation of the camera is synchronized with the shock tunnel flow using a trigger pulse generated by the pressure sensor located at the end of the tube. The light is switched on just before the experiment and only the camera is triggered to synchronize with the shock tunnel flow. The camera is focused on the region of interest, that is, near the cowl region to visualize the flow field resulted because of forebody/cowl shock interactions. The acquisition of data during experiment was done by using a NI PXI-6115 data acquisition system (manufactured by National Instruments Pvt. Ltd.) at a 10 MHz sampling rate.

The model is fixed to the top wall of the test section with the required ramp-cowl combination. All experiments are carried out at Mach 8 with dry air as the test gas. Typical freestream conditions are given in Table 1.

The model is supported by clamps and adjustable stings so that the cowl is attached to the forebody rigidly and the contraction ratio does not change during the run. A photograph of the model inside the facility is shown in Fig. 3.

The previous arrangements for safe testing of the model inside the tunnel raise doubt of the possibility of flow blocking because of their presence along with the model. To ensure that the model is subjected to steady flow during the test time of the tunnel, the ramp shock angle measured from the schlieren pictures recorded during the test time for a few runs is plotted in Fig. 4. It can be observed that, for all runs, the ramp shock angle remains steady except for the ~400 μs case which corresponds to the starting time of the nozzle. These measured angles compare well with the oblique shock angles corresponding to Mach 8 and ramp angle of 27 deg. This shows that in all runs, during the tunnel test time, the model is subjected to steady flow of Mach 8 for which it has been designed. This ensures that any unsteady flow features observed during the run is because of the flow pathology in the model.

In addition, for a run, the schlieren pictures are recorded during the test time and an intensity scan is performed along several lines for each figure to locate the exact location of the ramp shock. Figure 5 shows the intensity scans obtained this way using MATLAB 7.0.4 superimposed over each other. From the figure it is clear that the ramp shock does not oscillate much during the test time, which means the model experiences steady hypersonic flow during the test time. When the ramp shock is steady, then it indicates that the flow entering the inlet is steady. On the other hand, when the ramp shock oscillations are present in the flowfield, the classical SOL condition will not be satisfied at the designed Mach number. The Mach number of the flow that eventually enters the inlet will be altered drastically if the ramp shock oscillations are appreciable ahead of the cowl in a given flowfield. The ramp shock oscillations may also alter the ramp/cowl shock interaction patterns. Hence in this study initial experiments are carried out to ensure that for the ramp angle oscillations are virtually negligible during the steady-state shock tunnel testing.

IV. Results and Discussions

As discussed in the previous paragraphs the present study involves variation of cowl length and cowl angle keeping the chamber height constant. The results include schlieren flow visualization, heat transfer rate, and surface pressure measurement inside the chamber and numerical results.

A. Cowls of Different Lengths

Experiments are carried out for different lengths of cowl, namely, 131, and 141, and 151 mm apart from the designed length, 111 mm. It may be recalled here that a 111 mm cowl at 10 mm chamber height is the designed configuration of the model. Extending cowl upstream is a popular variable-geometry feature for it helps in recovering the spilled mass at off-design conditions. So it is important to understand the shock interaction phenomena when this feature is employed. For all these cowl lengths the chamber height is kept constant at 10 mm. Shock patterns obtained for these cases are discussed in the following paragraphs.

Figure 6 shows a set of sequential schlieren photographs obtained for 111-mm cowl configuration at design Mach number. The nozzle starting time, steady flow and flow termination can be clearly seen. From the schlieren pictures it can be seen that for this model configuration the SOL condition seems to be satisfied, that is, the forebody shock meets the cowl at its tip and is reflected back to the shoulder (clearly seen in the image that corresponds to 555 μs). But, however, this shock pattern does not last for the entire test time because the flow is not established in this case. This can be known by calculating the Kantrowitz limit [13]. It is a preliminary estimate of internal contraction for self-starting and is calculated by assuming a normal shock at the start of internal contraction and calculating a 1-D, isentropic internal area ratio that produces sonic flow at the throat.

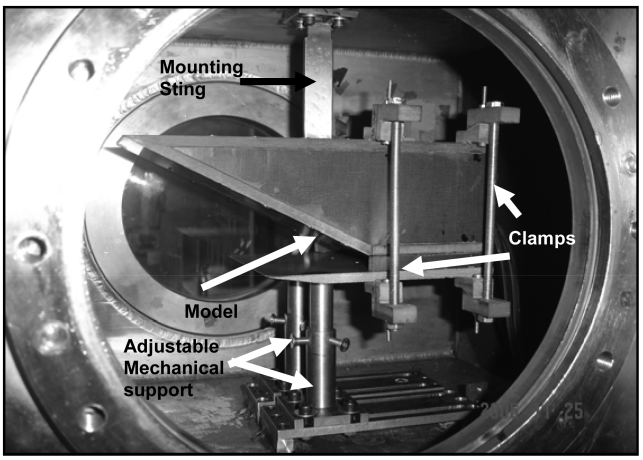

Fig. 3 Photograph of the model mounted inside the tunnel with the mechanical support.

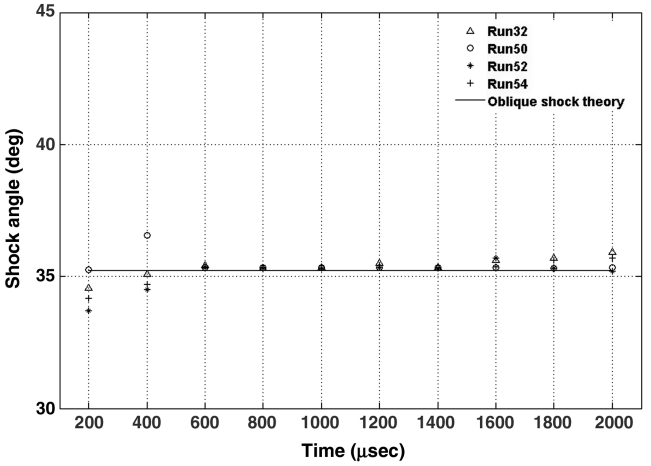

Fig. 4 Plot of the ramp shock angle (measured from Schlieren images) vs time.

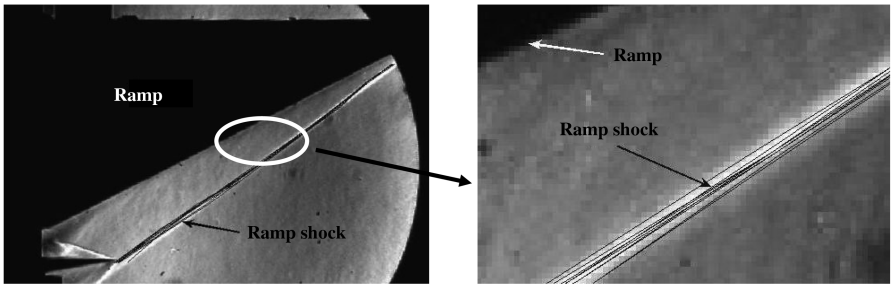

a) b)

Fig. 5 a) Shock locations obtained at different times during the test time of the tunnel superimposed over each other. b) Selected area magnified for a better view.

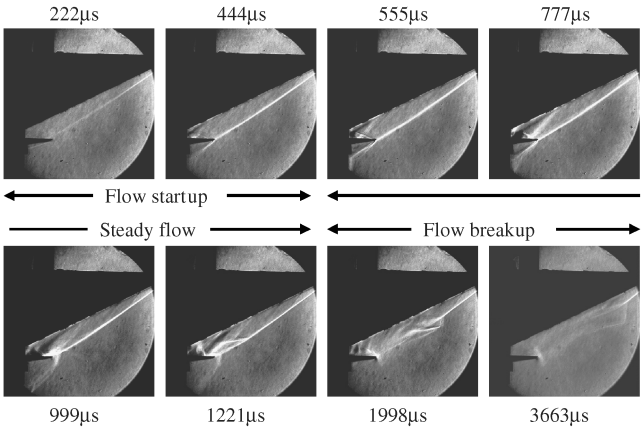

Fig. 6 Schlieren photographs of the flow development for 111 mm cowl at design condition.

Because a single normal shock is having more total pressure than a series of oblique shocks, an internal contraction ratio more than the Kantrowitz limit can also be tolerated. This means that by maintaining an internal contraction ratio less than or equal to the Kantrowitz limit the inlet can never unstart because of overcontraction. For the present case, the Kantrowitz limit is 1.62, whereas the internal contraction ratio (defined as the projected area of the inlet at the beginning of internal contraction) is 2.3. However, this value is intolerable here which means the inlet is overcontracted and hence the flow not established through it. Figure 7 shows the important flow features for this cowl configuration.

The adverse pressure gradient created by the cowl shock is strong enough to separate the ramp boundary layer. The separation shock is visible in the schlieren images which moves upstream of the ramp for the flow spillage taking place here. The shear layer is also visible. Numerical simulations are carried out concurrently using a commercial 3-D, compressible Navier–Stokes code (Ansys CFX 10), where freestream conditions obtained from the experiments are supplied as inputs to compliment the experimental findings. Because real gas effects can be negligible at this flow enthalpy, this code can be suitably used for the present study. The flow is assumed to be laminar for the simulation because the facility Reynolds number is $\sim 10^6$/m and the model length is 230 mm. The mesh used for the simulation is an hexahedral type and is generated using a commercial mesh generating code Ansys ICEM CFD 10. The results are second order accurate, grid independent, and convergent to an rms residual value of 10^{-5}. The separation bubble seen in the experiments is also captured numerically as shown in Fig. 8.

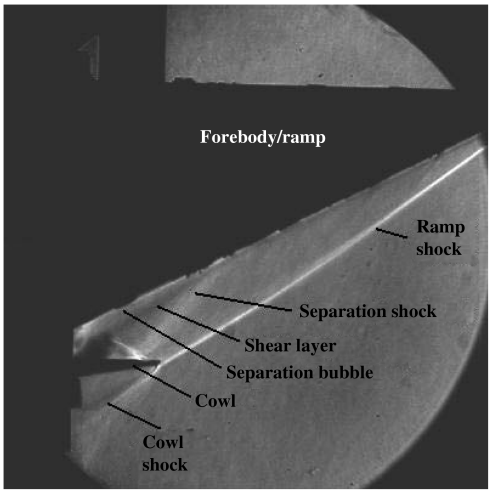

Fig. 7 Important flow features for 111 mm cowl at design condition.

Figure 9 shows sequential schlieren images for the 131-mm cowl case. The ramp shock and the cowl shock interact with each other to form an Edney type II interference pattern as described by Edney [14]. It is to be noted here that by carefully analyzing his experimental studies, Edney was able to identify six basic types of shock interference patterns depending upon the intensities and relative directions of the intersecting shocks. The type-I and type-II patterns form when two oblique shocks of opposite nature intersect each other. The type I interference is a regular reflection, whereas the type II interference is a Mach reflection. In the first two schlieren pictures from the steady time of the tunnel run the normal shock is clearly visible. This can be better understood with the help of Fig. 10, which shows the schlieren photograph from the visualization and the schematic of the Edney type II interference pattern side by side. The ramp shock, cowl shock, and the Mach stem are denoted by C_1, C_2, and C_5, respectively. The reflected shock from the first triple point and slip streams from the two triple points are also visible. Because here the inlet operates at an internal contraction ratio of 2.3, the flow gets choked like the previous case. The later two schlieren pictures from the steady time (Fig. 9) confirm the same. The Edney type-II interference pattern seen in two previous pictures now becomes a lambda pattern with a normal shock right before the inlet with a single triple point. The reflected shock going inside the chamber initially starts impinging on the ramp with the formation of the lambda pattern.

Figure 11 shows a series of schlieren pictures for a 141-mm cowl. The shock pattern obtained here is similar to the Edney type-II pattern obtained in 131-mm cowl case. One thing can be observed here that unlike the 131-mm case, the shock pattern remains undisturbed for the entire test time after which the lambda shock pattern forms. This can be attributed to the longer length of the cowl. The formed shock pattern will remain as it is unless there is enough spillage of air downward and sideways so that the shock system cannot be supported. So more cowl length means this process will take more time. The reflected shocks from both the triple points and both the slip streams are visible. The reflected shock from the first triple point (i.e., T_1 if this pattern is compared to the Edney type-II schematic in Fig. 10b) directly impinges on the ramp and the reflected shock from the second triple point goes into the chamber after undergoing one more reflection from the cowl plate.

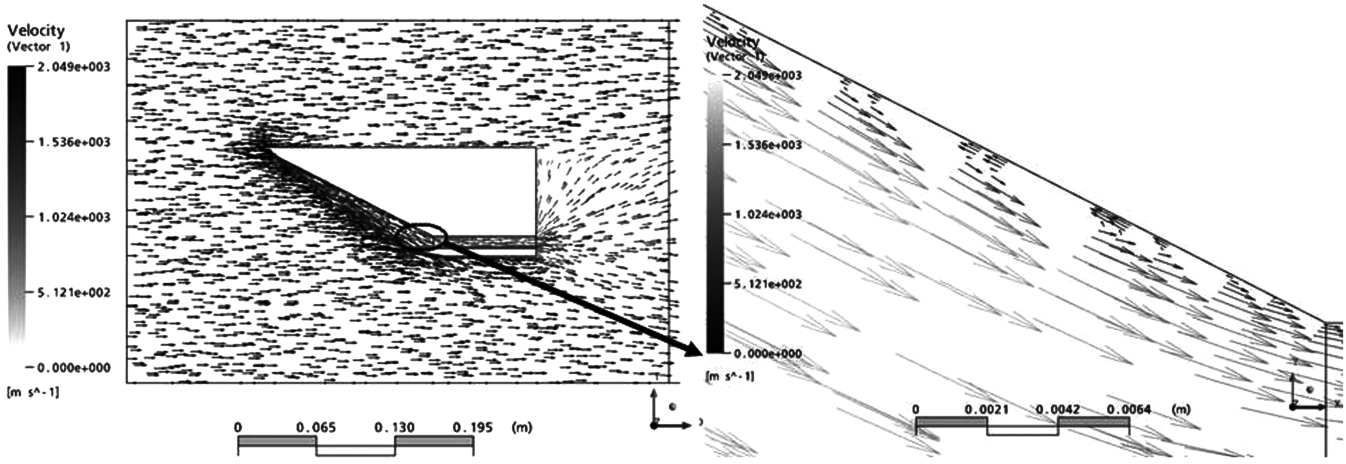

a) b)

Fig. 8 a) Velocity vector plot obtained numerically for 111 mm cowl at design condition. b) Selected region magnified to show the separation bubble.

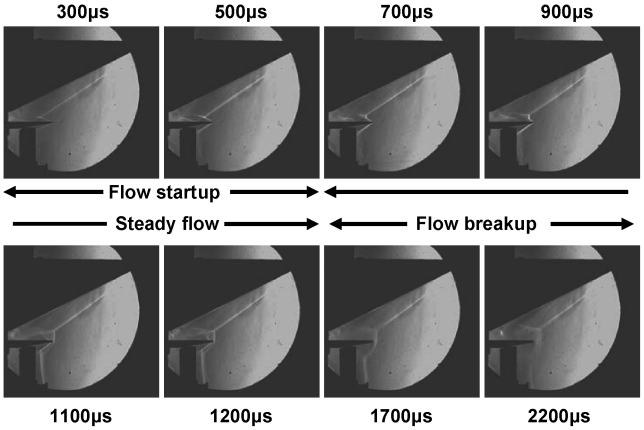

Fig. 9 Schlieren photographs of the flow development for 131 mm cowl at design condition.

Figure 12 shows a series of schlieren pictures for 151-mm cowl. The shock pattern formed here can be classified as Edney type-I interference if this shock pattern is compared with the schematic as shown in Fig. 13. The ramp shock C_1 and the cowl shock C_2 interact with each other with a single triple point T_1. The transmitted shock C_3 impinges on the ramp, whereas the other transmitted shock C_4 undergoes further reflection from the cowl plate and enters the chamber. The shock C_3 is strong enough to separate the ramp boundary layer and a weak separation shock is also visible in the schlieren images. From the steady time schlieren images it can be observed that this shock pattern remains till 916 μs after which the lambda shock pattern can be seen. A train of normal shocks moving upstream can also be seen in the last two schlieren pictures of the steady flow.

B. Cowls of Different Angles

Experiments are also conducted at different cowl angles (0, 10, and 20 deg) keeping the chamber height constant at 10 mm to study and understand the resulting shock patterns. "Rotation of a cowl" is a variable-geometry feature that can be adopted to operate the inlet at variable contraction ratios [5]. In the beginning the inlet can be operated at lower contraction ratios to ease the starting process. Once the inlet is started the contraction ratio can be increased. Because the test time in a shock tunnel is less ($\sim$1 ms in HST2), it is not possible to dynamically rotate the cowl during the steady-state run time. So it has been decided to perform experiments by fixing the cowl plate at different angles with reference to the freestream.

Figure 14 shows the schlieren images for a 10-deg cowl angle. The contraction ratio for this case is 7.9. It can be observed that the ramp shock impinges on the cowl tip and reflects back almost to the shoulder which means that the SOL condition is satisfied in this case. It can be seen from the schlieren pictures that this shock pattern

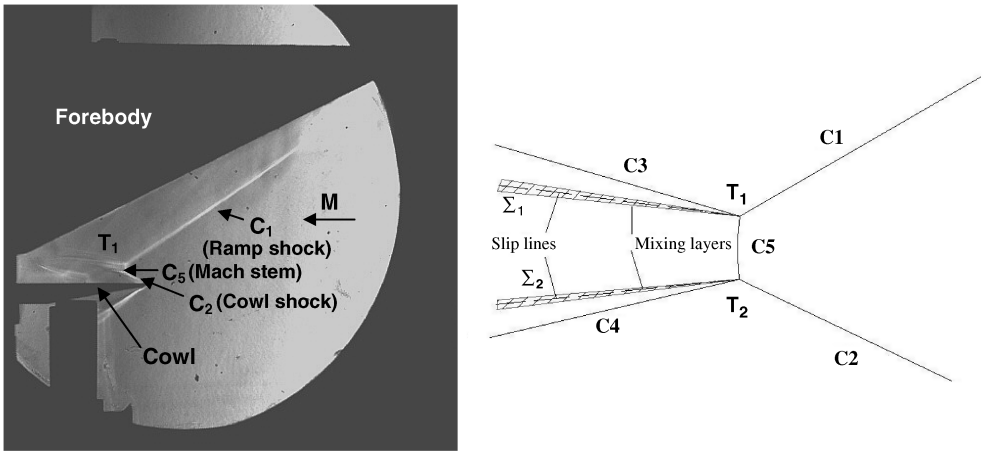

a) b)

Fig. 10 a) Schlieren photograph for 131 mm cowl during the test time of the tunnel showing the shock pattern. b) Schematic of Edney type-II shock interference.

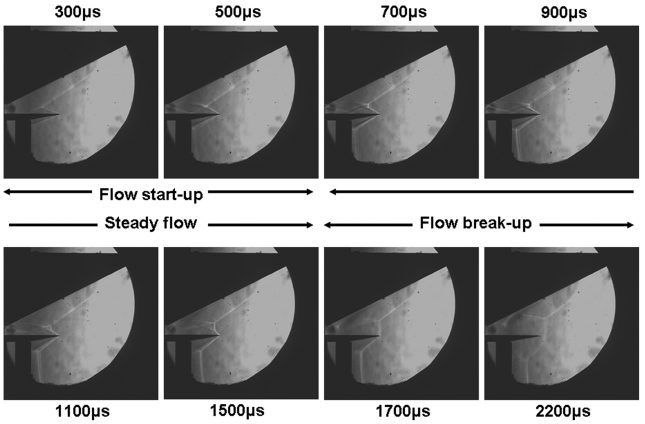

Fig. 11 Schlieren photographs of the flow development for 141 mm cowl.

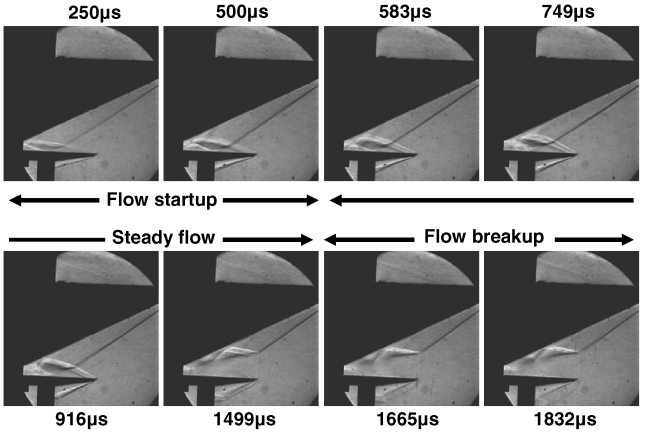

Fig. 12 Schlieren photographs of the flow development for 151 mm cowl.

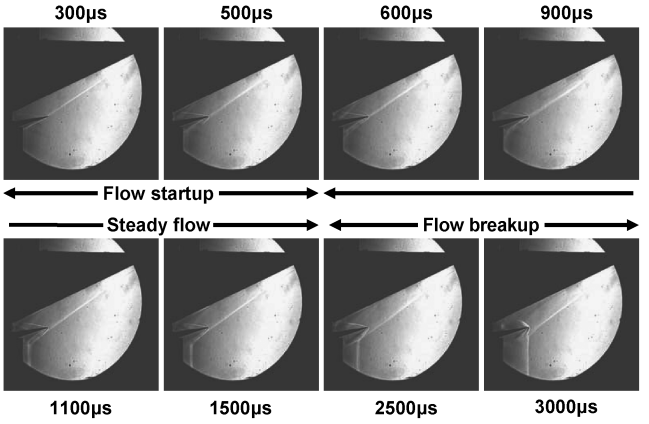

Fig. 14 Schlieren photographs of the flow development for 10 deg cowl.

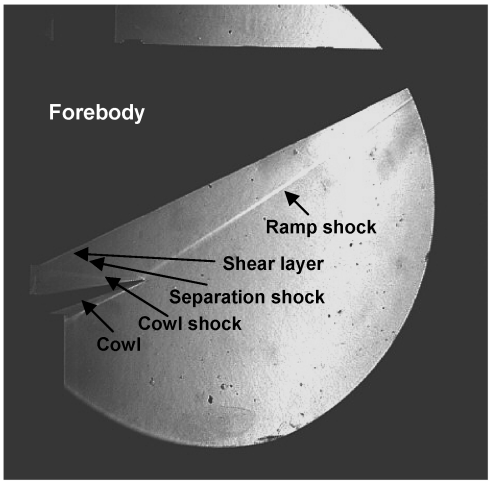

Fig. 15 Important flow features for 10 deg cowl at design condition.

remains almost the same during the entire duration of the test time. This means that the flow does not get choked and hence the flow through the inlet appears to have been established. This is unlike the 0-deg cowl case discussed in the previous paragraphs (see Fig. 6), where the flow was not established through the inlet.

The important flow features for the 10-deg cowl case are marked in Fig. 15. The reduction in contraction ratio leads to the establishment of the flow in this case. The separation shock and the separation bubble are visible in the schlieren pictures. The cowl shock and the separation shock interact with each other to form a possible Edney type-I interference. However, the slip stream emanating from the triple point is not visible in the picture.

Figure 16 shows the schlieren images for a 20-deg cowl angle. The contraction ratio for this case is 6.8. It can be observed from the schlieren images that the ramp shock impinges on the cowl tip and the reflected shock goes into the chamber. The cowl shock, however, impinges on the ramp surface and undergoes a series of reflections before finally entering the chamber. Like the previous case, here too

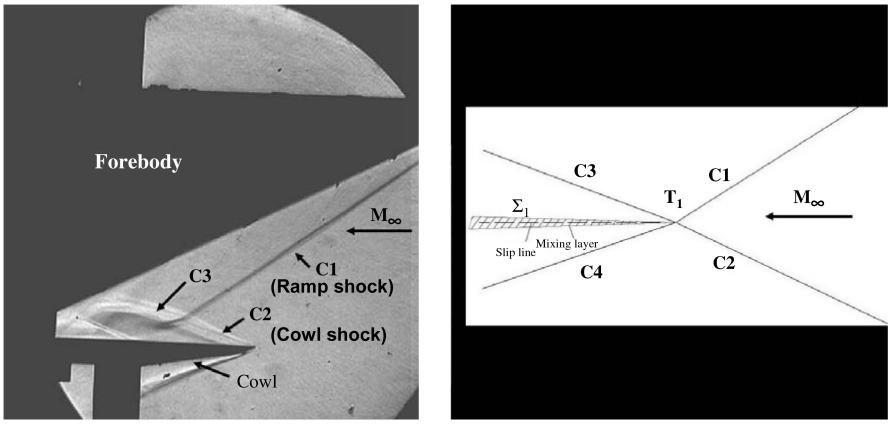

a) b)

Fig. 13 a) Schlieren photograph for 151 mm cowl during the test time of the tunnel showing the shock pattern. b) Schematic of Edney type-I shock interference.

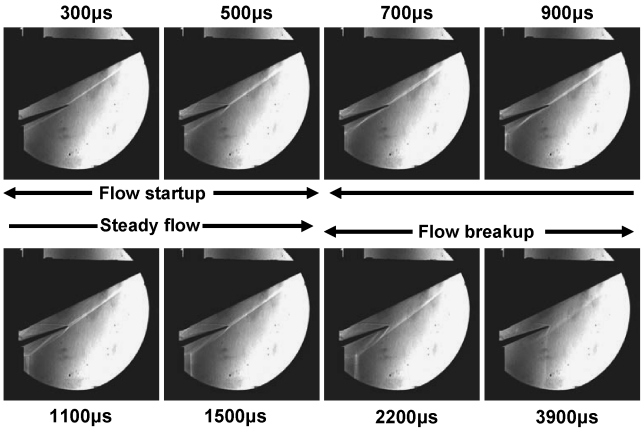

Fig. 16 Schlieren photographs of the flow development for 20 deg cowl.

this shock pattern remains in this state for the test time and does not move upstream as seen with a 0 deg cowl described in the previous paragraphs. Hence in this case it appears that the flow is established through the inlet. The important flow features for this case are similar to the 10-deg cowl case and can be better understood with the help of Fig. 15 (given for a 10 deg cowl), except for the location of cowl shock impingement and separation bubble.

The shock patterns are also obtained from the steady numerical simulations performed in parallel for the above cowl configurations, that is, for different cowl angles keeping the other geometric parameters unchanged. This is done to observe the shock pattern inside the chamber because the flow visualization experiments are confined to the cowl region only. Figure 16 shows the numerical shock patterns obtained for the above configurations. It can be seen in Fig. 17a that at 0 deg cowl, a normal shock appears inside the chamber which is indicative of the fact that flow is not established through it. For Figs. 17b and 17c, that is, for cowl angles of 10 and 20 deg, respectively, a series of oblique shock can be seen inside the chamber which means flow is established and is supersonic inside it. This is consistent with the experimental findings.

C. Measurement of Static Pressure and Heat Transfer Rate Inside the Chamber

The flow visualization studies performed in the present investigation are confined to the region in front of the cowl only because the primary interest was to study the ramp/cowl shock interaction. To understand the flow physics inside the chamber because of the shock interactions around the cowl region, point measurements like static pressure and heat transfer rate are performed inside the chamber for the cowl configurations described in this paper. Figure 18 shows the schematic of the model showing the locations of these sensors.

Figure 19a shows the pressure values measured experimentally and the distribution of pressure obtained numerically along the length of the chamber for all lengths of cowl. As seen in the schlieren images, in case of 111 mm cowl the cowl shock and reflected ramp shock impinges on the shoulder of the model and possibly interacts with the expansion fan created at the shoulder region. But this pattern does not last for long, as the flow gets choked. For both 131 and 141 mm an Edney type-II shock interference pattern is formed

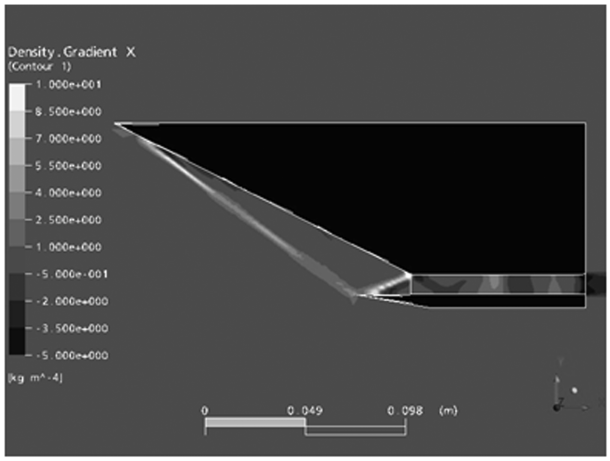

a)

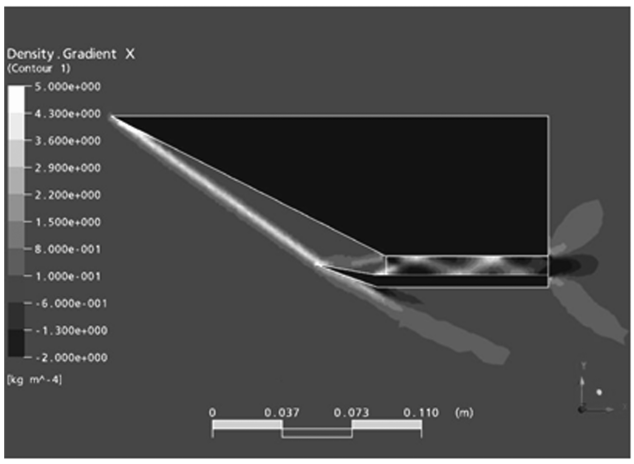

b)

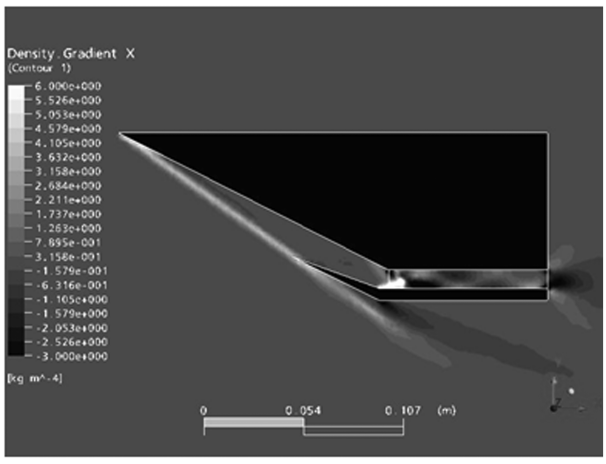

c)

Fig. 17 Shock patterns obtained from numerical simulation for cowls of different angles at a) 0 deg, b) 10 deg, and c) 20 deg.

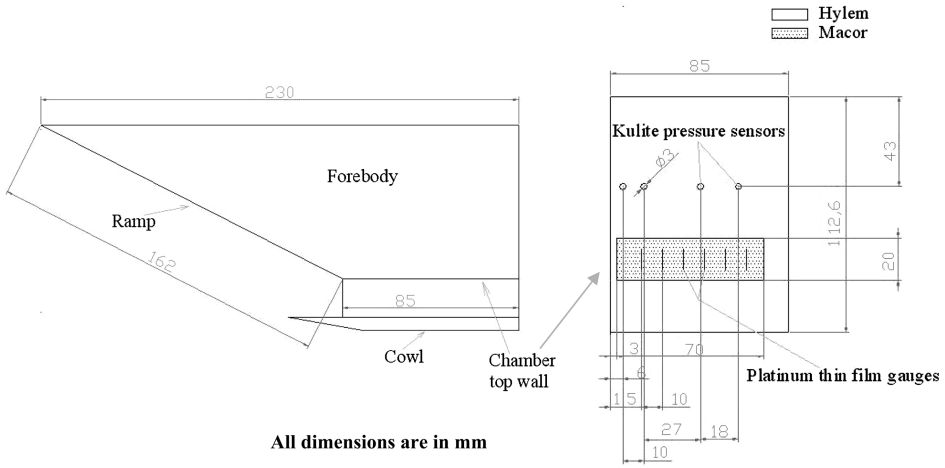

Fig. 18 Schematic showing the sensor locations inside the chamber.

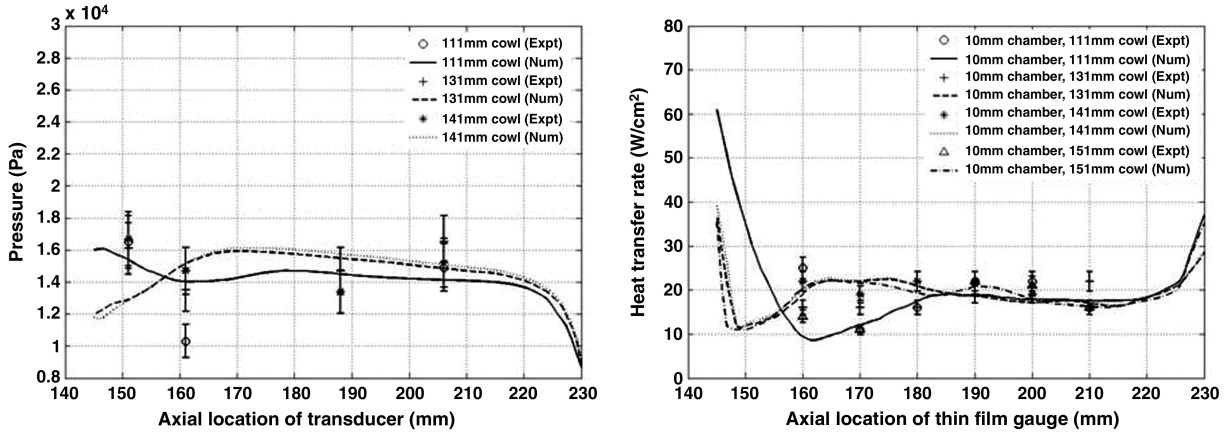

a) b)

Fig. 19 Experimentally measured values and numerically obtained distribution of a) static pressure, and b) heat transfer rate, along the length of the chamber for different lengths of cowl.

because of the ramp shock/cowl shock interaction. It is worthwhile to recall here that the flow is not established in all three cases (overcontracted and flow gets spilled). So the shock pattern formed during the beginning of the run will continue to remain so unless there is enough mass spillage downward and sideways and the formation of shocks is not supported further. Though the Mach stem locations in both the cases are slightly different from each other, the reflected shocks in both cases enter into the chamber after undergoing further reflections. Because the contraction ratio is the same in all these cases the measured values inside the chamber will be a strong function of the shock–shock interactions. The first sensor for all cowl lengths shows a higher value of pressure, which means this sensor is located at a region if a reflected shock impinges on the inlet chamber. The low value of pressure shown by sensor 2 for the 111-mm cowl case could be due to the centered expansion fan at the shoulder.

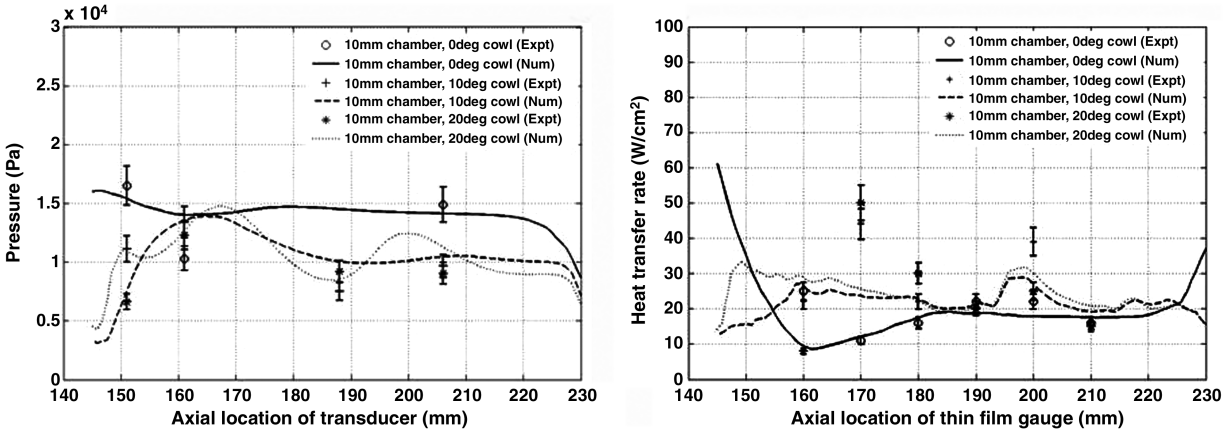

a) b)

Fig. 20 Experimentally measured values and numerically obtained distribution of a) static pressure, and b) heat transfer rate, along the length of the chamber for different angles of cowl.

Figure 19b shows the heat transfer values measured experimentally and the distribution of heat transfer rate obtained numerically along the length of the chamber for different lengths of cowl tested. The first sensor shows the highest heat transfer value ($\sim$25 W/cm^2) for the 111-mm cowl case. It is followed by 131 and 141-mm cases and then a 151-mm cowl case. It may be recalled here that in the case of 131 and 141-mm cowl cases, an Edney type-II interference is observed, whereas in the 151-mm case it is an Edney type-I interference. Because the flow gets choked in all the cases the average heat transfer rate ($\sim$20 W/cm^2) inside the chamber does not vary much as observed from subsequent sensor readings.

Figure 20a shows the pressure values measured experimentally and the distribution of pressure obtained numerically along the length of the chamber for three angles of cowl, namely, 0, 10, and 20 deg keeping the chamber height at 10 mm. It can be recalled here that the flow through the inlet is not established in the 0 deg case, whereas in the other two cases the flow is established in the inlet. The geometric contraction ratios for these two cases are found to be 7.9 and 6.8, respectively. The pressure value recorded in the first sensor, that is, the one close to the throat region shows the highest value for the 0 deg case because the contraction ratio is maximum here. The sudden rise of pressure from the first sensor compared to the second for the 20-deg angle case essentially shows the location of impingement of cowl reflected shock.

Figure 20b shows the heat transfer values measured experimentally and the distribution of heat transfer rate obtained numerically along the length of the chamber for a 10-mm chamber height with different cowl angles. As discussed in the previous paragraphs, for the 0 deg case the flow is choked and the flow through the inlet did not start, whereas in the other two cases the flow through the inlet is established. The heat transfer rate value shown in the first sensor is more in the 0 deg case where the CR is more. The peak values of heat transfer rate at 170 and 200 mm show the possible locations of shock impingement.

V. Conclusions

This paper describes the experimental and numerical investigation to study the ramp/cowl shock interaction processes for two geometrical variations: namely, the variation of the cowl length and the cowl angle. A 2-D, planar, single ramp scramjet inlet model has been designed, fabricated, and tested for the above investigation. The experiments are conducted for four lengths of cowl, namely, 111, 131, 141, and 151 mm and three cowl angles, namely, 0, 10, and 20 deg keeping other geometrical parameters constant. All experiments are carried out in the IISc hypersonic shock tunnel, HST2, at a nominal Mach number of 8.0. Time-resolved schlieren visualization is performed to observe the shock interaction near the cowl region. Different cowl lengths and angles result in different flow morphologies as observed in the schlieren images. For the 111 mm cowl a strong separation bubble is seen near the shoulder region. Both 131 and 141 mm cowl showed Edney's type-II interference, whereas 151 mm showed Edney's type-I pattern. In all, the flow is choked because of a high contraction ratio. So these shock patterns do not last for the entire test time, but rather become a lamda pattern toward the end. The average heat transfer rates of the last four heat transfer gauges (180, 190, 200, and 210 mm from the forebody tip) for all lengths of cowls tested are found to be almost the same ($\sim$20 W/cm^2). This is because the flow is choked in all these cases. The numerical simulation also shows uniform distribution here, consistent with the experimental findings. From experiments with different cowl angles it is observed from the visualization that increasing the cowl angle reduces the geometric CR which helps the flow inside the inlet get established. For 0 deg cowl the maximum pressure value recorded is $\sim 1.7 \times 10^4$ Pa, whereas for 10 and 20 deg cowl it is $\sim 1.1 \times 10^4$ Pa and $\sim 1.2 \times 10^4$ Pa, respectively, which is because of the higher contraction ratio. The locations of heat transfer peaks for 10 deg cowl at design condition can be observed to be occurring at 170 and 200 mm from the forebody tip having values $\sim$44 and $\sim$39 W/cm^2, respectively. For a 20 deg cowl they seem to be occurring at 170 and 180 mm from the forebody tip having values of $\sim$50 and $\sim$30 W/cm^2. These locations indicate the likely locations of shock impingements inside the chamber. With the evolution of the concept of upstream fuel injection in recent times these may the most appropriate locations for fuel injection. However, flow visualization inside the chamber could show the accurate locations of shock impingements and reveal more on the shock dynamics inside it.

Acknowledgments

The authors acknowledge the help and support extended by the High Enthalpy Aerodynamics (HEA) lab staff and students for their help during the experiments. The authors would like to thank the Indian Space Research Organization (ISRO) Space Technology cell, Indian Institute of Science, Bangalore, for financially supporting this project [ISRO Space Technology Cell (ISTC) 207]. The authors would also like to thank the technical staff of High Enthalpy Aerodynamics Laboratory for all the help during the experiments.

References

[1] Falempin, F., and Wendling, F., "Experimental Investigation of Starting Process for a Variable Geometry Air Inlet Operating from Mach 2 to Mach 8," AIAA Paper 2006-4513, July 2006.

[2] Mrozinski, D. P., and Hayes, J. R., "Numerical and Experimental Analysis of a Hypersonic Variable Geometry Inlet," AIAA Paper 99-0899, Jan. 1999.

[3] Marquart, E. J., "Predictions and Measurements of Internal and External Flow Field of a Generic Hypersonic Inlet," AIAA Paper 91-3320, Sept. 1991.

[4] Tani, K., Kanda, T., and Kudo, K., "Effect of Side Spillage from Airframe on Scramjet Inlet Performance," NAL TR-1409T, 2000.

[5] Bedarev, I. A., Fedorova, N. N., Goldfeld, M. A., and Falempin, F., "Mathematical Modeling of Supersonic Turbulent Flows in Inlets with Rotating Cowl," *Proceedings of the Third International Conference on Computational Fluid Dynamics, ICCFD3*, Springer, Berlin/Heidelberg, 12–16 July 2004, pp. 295–300.

[6] Kanda, T., Komuro, T., Masuya, G., Kudo, K., Murakomi, A., Tani, K., Wakamatsu, Y., and Chinzei, N., "Mach 4 Testing of Scramjet Inlet Models," *Journal of Propulsion and Power*, Vol. 7, No. 2, 1991, pp. 275–280. doi:10.2514/3.23321

[7] Holland, S. D., "Reynolds Number and Cowl Position Effects for a Generic Sidewall Compression Scramjet Inlet at Mach 10: A Computational and Experimental Investigation," AIAA Paper 92-4026, 6–8 July 1992.

[8] Van Wie, D. M., and Ault, D. A., "Internal Flow Field Characteristics of a Scramjet Inlet at Mach 10," *Journal of Propulsion and Power*, Vol. 12, No. 1, 1996, pp. 158–164. doi:10.2514/3.24005

[9] Boon, S., and Hillier, R., "Hypersonic Inlet Flow Analysis at Mach 5,6 and 7," AIAA Paper 2006-12, 9–12 Jan. 2006.

[10] Mouton, C. A., and Hornung, H. G., "Experiments on the Mechanism of Inducing Transition Between Regular and Mach Reflection," *Physics of Fluids*, Vol. 20, No. 12, 2008, p. 126103. doi:10.1063/1.3042261

[11] Satheesh, K., Jagadeesh, G., Reddy, K. P. J., "High Speed Schlieren Facility for Visualization of Flow Fields in Hypersonic Shock Tunnels," *Current Science*, Vol. 92, No. 1, 2007, pp. 56–60.

[12] Schultz D. L, and Jones T. V., "Heat Transfer Measurements in Short-Duration Hypersonic Facilities," AGARDograph AG-165, 1973.

[13] Kantrowitz, A., and Donaldson, C., "Preliminary Investigations of Supersonic Diffuser," duP, NACA WR L 713, May 1945.

[14] Edney, B., "Anomalous Heat Transfer and Pressure Distributions on Blunt Bodies at Hypersonic Speeds in the Presence of an Impinging Shock," Aeronautical Research Institute of Sweden, FFA Rept. 115, 1968.

K. Asai
Associate Editor